FERMILAB-CONF-04-253-TD

Magnetic Instabilities in Nb_3Sn Strands and Cables

Vadim V. Kashikhin and Alexander V. Zlobin

Abstract—This paper describes a model for calculation of magnetic instabilities in superconducting wires with transport current and reports results of instability simulations in Nb_3Sn strands from different manufactures. The effect of magnetic instabilities on the strand and cable performance is presented and a criterion for the maximum effective sub-element size of strands for high field magnets is formulated.

***Index Terms*—Superconducting accelerator magnets, superconducting filaments and wires, magnetic fields.**

I. Introduction

Several Nb_3Sn shell-type dipole magnets and mirror models built at Fermilab using 1-mm MJR strand had quenches at ~50÷60% of the expected critical current [1]-[2]. Different possible causes, including the splice heating, mechanical damage and some others, intended to explain the magnet performance were proposed, evaluated and rejected in the course of work due to inconsistency with the experimental data. The further experimental studies and thorough analysis performed on the magnets, including quench origin and quench propagation velocity, critical current and critical temperature measurements in the magnet coil, pointed on the instabilities in superconducting strands.

It is well known that the performance of superconducting wires, cables and magnets can suffer from magnetic instabilities associated with rapid motion of magnetic flux trapped inside the filaments. These instabilities or flux jumps depend mainly on the critical current density of superconductor, effective filament size, specific heat, and cooling conditions.

Decades ago, the stability issue was addressed for NbTi and Nb_3Sn wires by reducing their effective filament diameter to 3÷10 microns. However, the new generation of Nb_3Sn wires produced for application in high field accelerator magnets have higher critical current densities (2÷3 kA/mm^2 at 12T and 4.2K) and relatively large, due to technological and economical reasons, effective sub-element sizes (50÷300 μm) that makes them potentially unstable.

Manuscript received October 4, 2004. This work was supported by the U.S. Department of Energy.

V.V. Kashikhin and A.V. Zlobin are with the Fermi National Accelerator Laboratory, m.s. 316, P.O. Box 500, Batavia, IL 60510 USA (corresponding author's phone: 630-840-6546; fax: 630-840-3369; e-mail: vadim@ fnal.gov).

The first rough estimation of the energy released during the flux jumps in the high-performance conductors was done based on the measured magnetization curve of MJR strand [3]. It revealed that the flux jumps in modern Nb_3Sn strands release considerable amounts of energy (comparable to the minimum quench energy) at low fields that may cause a magnet quench. This analysis triggered a series of the short sample tests aimed at the assessment of the strand performance in the low field region. The first experimental results confirmed that the strand critical currents at low fields are indeed limited at 15÷20% of the expected values [4]. It stimulated the development of a detailed numerical model for the quantitative analysis of the magnetic instabilities in superconducting strands, cables and magnets.

II. Model Description and Results

The general concept of the magnetic instabilities in superconductors is vastly described in literature. The criterions of adiabatic stability for a superconducting plate are formulated in [5]-[6]:

$$J_c^2 a^2 < \frac{3}{\mu_0}\gamma C(-J_c \partial J_c / \partial T) \quad \text{or} \quad \frac{\mu_0 J_c^2 a^2}{\gamma C(T_c - T_0)} = \beta < 3 \cdot$$

For the typical Nb_3Sn MJR strand parameters J_c = 18000A/mm^2, γC = 1.7mJ/cm^{3}K, T_c = 17.5K and $-J_c/(\partial J_c/\partial T)$ = 16.5K at 1T background field and the bath temperature T_0 = 4.2K, the above criteria limit the maximum filament sizes to 28μm and 24μm correspondingly. Nevertheless, some Nb_3Sn magnets made of strands with the effective sub-element sizes in excess of 50÷100μm, reached their short sample limits in the close to adiabatic conditions [7]-[9].

It is obvious, that the simple differential criterions of adiabatic stability in the vicinity of T_0 need improvements to adequately describe the maximum effective filament size for the Nb_3Sn magnets and to explain different quench performances of magnets made from similar conductors. Thus, further efforts were undertaken for the analysis of the stability issues in the modern Nb_3Sn superconducting strands.

A. Assumptions and simplifications

The analysis is based on the *critical state model* [10] with the critical current density as a function of the background field only. The temperature was assumed to be uniform within a strand that is the case for the magnetic diffusivity being larger than the thermal diffusivity. This simplification imposes

certain restrictions on the model applicability. It was also assumed that heat generated in superconductor increases its internal energy without changes in the volume and pressure. For simplicity, the round filaments were approximated with squares of the same area. The problem was solved for a plate using the following one-dimensional set of constrains: $I_x = I_y = 0$, $I_z \neq 0$; $B_x = B_z = 0$, $B_y \neq 0$; $E_x = E_y = 0$, $E_z \neq 0$.

B. Current and magnetic field profiles inside a SC filament

There are three components of the magnetic field inside a filament: the background field, the field from the persistent currents induced during the background field change and the field from the transport current. Fig. 1 gives examples of the normalized current density and magnetic field profiles inside a 100μm SC filament for different background fields and transport currents, computed by the Ampere's law. The critical current density in the filament was parameterized according to [11] with an additional self-field correction to provide the best fit for the critical current derived from the magnetization measured on MJR strands [12]. Depending on the background field, transport current and flux penetration history, there can be different current and field profiles inside a filament.

Since the critical current density in superconductor depends on the temperature - the current and field distributions inside a filament are also functions of the temperature. Fig. 2 (left) gives examples of the magnetic field profiles inside the filament for different temperature variations ΔT over T_0.

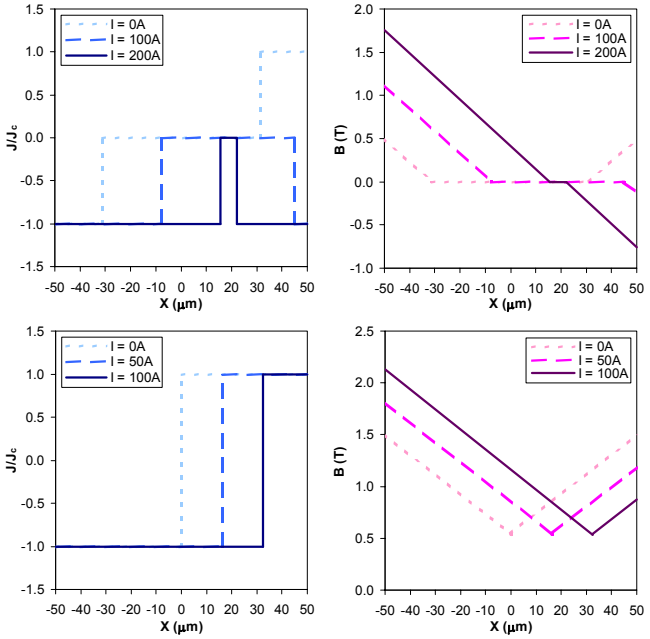

Figure 1. Normalized current density and magnetic flux density for the background fields of 0.5 T (top) and 1.5 T (bottom).

C. Heat generation during a flux change

A temperature variation inside superconducting filament results in the magnetic flux change. According to the Faraday's law, variation of the magnetic flux generates the electric field:

$$\oint \vec{E} d\vec{l} = -\frac{d\Phi}{dt}.$$

For the one-dimensional problem constrains, it can be written in the following form:

$$\left(E_z(T_0,\Delta T,x) + E_z(T_0,\Delta T,0)\right)dt = -\left(B_y(T_0+\Delta T,x) - B_y(T_0,x)\right)dx.$$

Integration of this equation over x coordinate yields the time integral of the electric field:

$$E_z^*(T_0,\Delta T,x) = -\int_0^x \left(B_y(T_0+\Delta T,x) - B_y(T_0,x)\right)dx - E_z^*(T_0,\Delta T,0).$$

Fig. 2 (right) gives an example of the electric field integral inside a filament due to the magnetic flux variation shown in Fig. 2 (left) caused by the temperature rise.

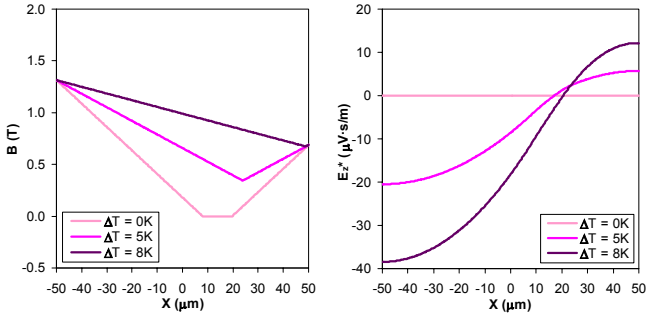

Figure 2. Magnetic flux density and electric field integral for the background field of 1T and the transport current of 50A.

Calculation of the energy released in a filament due to magnetic flux change can be performed by several ways [5]-[6]. We have chosen the approach based on the Poynting vector $\vec{S} = \vec{E} \times \vec{H}$. The total power of the electromagnetic energy flow through the surface surrounding a closed volume equals to the volume integral of the sum of the resistive loss power and time derivatives of the energies stored in the electric and magnetic fields inside that volume:

$$\oint_{Surface} (\vec{E} \times \vec{H}) \cdot d\vec{s} = -\int_{Volume} \left[\left(\vec{E} \cdot \vec{J}\right) + \frac{\partial}{\partial t}\left(\varepsilon \frac{E^2}{2} + \mu \frac{H^2}{2} \right) \right] dv.$$

Integrating both parts of this equation over time and for the one-dimensional problem yields:

$$\oint_{Surface} E_z^* H_y ds = \int_{Volume} \left(\Delta Q + \Delta W_e + \Delta W_m\right) dv,$$

where ΔQ is the increment of the heat dissipations and ΔW_e ΔW_m are the increments of the energies stored in the electric and magnetic fields inside the volume.

The value of the energy stored in the electric field is much smaller than the one stored in the magnetic field for any reasonable parameter variations in the given problem and is neglected. Averaging the heat dissipation and stored energy over the filament cross-section yields the following simple expression for the heat dissipation:

$$\Delta Q = \frac{1}{2a}\left|_{-a}^{a} E_z^* H_y - \Delta \overline{W}_m.\right.$$

This formula allows analytical calculation of the energy released in a filament based on the initial and final states of the current and magnetic field independently of time.

D. Instabilities in a strand without the transport current

The increment of the internal energy ΔU associated with the ΔT is determined by:

$$\Delta U(B,T_0,\Delta T)=\int_{T_0}^{T_0+\Delta T} C_p(B,T)dT\cdot$$

The total specific heat of a strand C_p is calculated as a sum of the specific heats of Nb_3Sn and Cu (in the stabilizer and matrix) averaged over the strand area. The specific heats of the Nb_3Sn and Cu were taken from [13]-[14] as volumetric functions of the temperature and (in case of the Nb_3Sn) the field.

Fig. 3 shows the heat dissipations due to the magnetic flux motion and the corresponding internal energies in the 1-mm MJR (D_{eff} = 110μm) and PIT strands (D_{eff} = 53μm) with the parameters given in [12] as functions of the temperature increment ΔT.

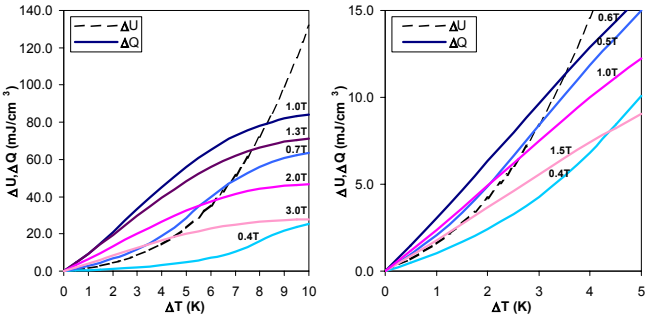

Figure 3. Heat dissipation and internal energy in 1-mm MJR (left) and PIT (right) strands for different background fields at I = 0. Note: variation of ΔU under the background field change is not shown due to its small effect.

As it follows from Fig. 3, the heat dissipation grows up with the background magnetic field until it reaches the maximum at the field close to the full penetration field for given conductor and then reduces with further increase of the field.

At some value of the background field, ΔQ overcomes ΔU in the vicinity of T_0. When it happens, a small temperature perturbation causes the flux motion that releases amount of heat exceeding the one that can be contained in the form of the internal energy, therefore the temperature-energy rise avalanche will continue until the amount of heat dissipated equals the internal energy:

$$\Delta Q(B,T_0,\Delta T_e)=\Delta U(B,T_0,\Delta T_e),$$

where ΔT_e is the temperature increment of the equilibrium.

Based on the data in Fig. 3, the field region corresponding to the unstable conditions for the MJR strand is 0.7÷3T and for the PIT strand is 0.5÷1.5T.

Magnetic instabilities in strands without the transport current are observed during the magnetization measurements. The calculated above field ranges, where instabilities occur, are in a good agreement with the regions of the flux jumps observed in the measured magnetization curves for the relevant strands [12]. It serves as the model verification without the transport current.

E. Instabilities in a strand with the transport current

Presence of the transport current in a strand violates the flux symmetry with respect to the filament center that results in larger electric field, as shown in Fig. 1-2. Also, it limits the equilibrium temperature by the strand critical temperature at a given field and current, after which the resistive heat generation takes place. Fig. 4 presents the heat dissipation and internal energy in the 1-mm MJR strand with the transport current.

The abrupt drop to zero in the heat generation curves denotes the critical temperature with an increment ΔT_c. According to the theories of the flux jump initiation in superconducting wires [15]-[16], there is always a probability of a flux jump that will follow the curves shown.

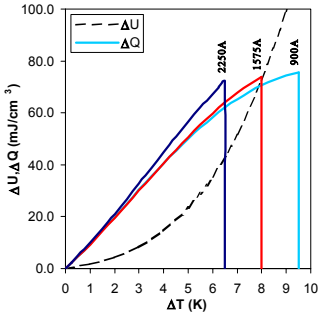

Figure 4. Heat dissipation and internal energy in MJR strand for different transport currents at 1T background field.

Obviously, if $\Delta T_c<\Delta T_e$ for a given background field and transport current, the flux jump will bring the conductor above the critical surface. Then the criterion of strand adiabatic stability can be written as:

$$\Delta Q(B,I,T_0,\Delta T_c(B,I,T_0))<\Delta U(B,T_0,\Delta T_c(B,I,T_0)),$$

and the maximum transport current strand can carry without the resistive transition I_{rt} should satisfy the following equation:

$$\Delta Q(B,I_c,T_0,\Delta T_c(B,I_{rt},T_0))=\Delta U(B,T_0,\Delta T_c(B,I_{rt},T_0)).$$

Instabilities in a strand with the transport current limit the maximum value of current strand can carry at given external conditions. Fig. 5 (left) shows the current of the resistive transition calculated for the 1-mm MJR strand as functions of the background magnetic field.

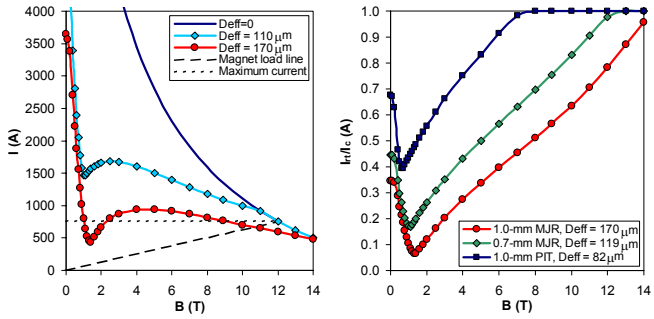

Figure 5. Current of the resistive transition and critical current of the 1-mm MJR strand in cable (left) and normalized maximum transport current for different cabled strands (right) calculated in adiabatic conditions.

The line for D_{eff} = 0 represents the critical current $I_c(B)$

strand would carry without instabilities. Based on observations of the sub-element deformation after the cabling [17], the average effective sub-element size is 170μm for the cabled strands with respect to 110μm for the round ones.

One can see that due to the instabilities, strand can carry only a fraction of the critical current, especially at low fields, where is a local minimum on $I_{rt}(B)$ curve at ~1.5T. The critical current at higher fields is not dramatically degraded that may seem acceptable for a high field magnet, however due to the magnetic flux return through the coil, virtually any accelerator magnet of either shell or block type has a region with wires exposed to the low fields. Therefore, the low-field minimum on the critical current curve defines the actual quench current that according to Fig. 5 (left) is 439A per strand or 12.3 kA for a 28-strand cable.

This number is in the middle of the quench current band achieved in the Fermilab shell type dipoles using the 28-strand cable [1]-[2]. There is also a good correlation of this current with the measurements performed on impregnated cable samples [18-19].

F. *Effects of the D_{eff} and J_c*

Fig. 5 (right) shows the $I_{rt}(B)$ for 0.7-mm and 1-mm MJR and 1-mm PIT strands with different effective sub-element sizes and the deformation ratio of sub-elements 1.55, normalized to the strands $I_c(B)$ as functions of the magnetic field. Reduction of the MJR strand diameter from 1-mm to 0.7-mm corresponding to the reduction of D_{eff} from 170μm to 119μm increases stability at low fields by more than a factor of two. Due to even smaller D_{eff}, the 1-mm PIT strand is a factor of five more stable than 1-mm MJR strand at low fields.

A magnet's ability to achieve the designed field depends not only on the minimum on $I_{rt}(B)$ curve, but also on the magnet load line that is a function of J_c and peak field in the coil B_{peak}. Fig 6. shows the maximum D_{eff} of (undeformed) sub-elements that are marginally stable under adiabatic conditions in a magnet based on round strands (solenoid) or Rutherford type cable as a function of the strand critical current density. These results are correct for MJR and PIT strands considered above, but may change for other wires, depending on the strand design.

It should be noted that depending on the *RRR* of Cu, the dynamic heat transfer, not included in this model, might improve the conductor stability and thus soften the D_{eff} requirements, however the experience with MJR strands does not justify relying on that.

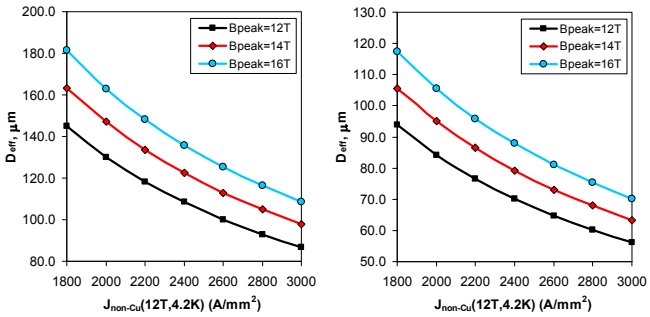

Figure 6. Effective sub-element diameter as a function of the critical current density for different projected fields in a coil for the round strand (left) and deformed with 1.55 ratio, corresponding to the Rutherford type cable (right).

CONCLUSION

An adiabatic model for simulation of magnetic instabilities in Nb_3Sn strands and cables has been developed. The model predicted significant reduction of the current carrying capability in the state of the art Nb_3Sn strands and cables with large D_{eff} and high J_c at low fields.

It has led to a quantitative explanation of the premature quenches in some Nb_3Sn magnets based on MJR conductor tested at Fermilab and elsewhere. It has also justified using of the more stable PIT conductor, which resulted in reaching the short sample limits in several Nb_3Sn magnets recently fabricated and tested at Fermilab [20].

The criterions for marginally stable strands were developed that can be used in magnet designs and in conductor development programs.

REFERENCES

[1] N. Andreev et al., "Development and test of single-bore cos-theta Nb_3Sn dipole models with cold iron yoke", *MT-17, IEEE Trans. Appl. Supercon.*, vol.12, no. 2, March 2002, pp.332-335.
[2] S. Feher et al., "Test results of shell-type Nb_3Sn dipole coils", *MT-18*, October 2003, Japan.
[3] V.V. Kashikhin, "Flux Jumps in Nb_3Sn magnets", Fermilab internal note, TD-03-005, January 2003.
[4] E. Barzi, Superconductor and Cable R&D for High Field Accelerator Magnets at Fermilab, Fermilab internal note, TD-04-024, June 2004.
[5] H. Brechna, *Superconducting magnet systems*, Springer, Berlin, 1973.
[6] M.N. Wilson, *Superconducting magnets*, Clarendon Press, Oxford, 1983.
[7] A. denOuden et al., "Application of Nb3Sn superconductors in accelerator magnets", *IEEE Trans. on Appl. Supercon.*, v.7, 1997
[8] A. McInturff et al., "Test results for a high field (13T) Nb_3Sn dipole", *Proc. Particle Accelerator Conf.*, Vancouver, Canada, 1997, p.3212.
[9] L. Chiesa *et al*., "Performance comparison of Nb_3Sn magnets at LBNL", *IEEE Trans. Appl. Supercon*., vol.13, no.2, June 2003, pp. 1254 – 1257.
[10] C.P. Bean, "Magnetization of high-field superconductors", *Review of Modern Physics*, vol. 36, no. 1, 1964, pp. 31-39.
[11] L.T. Summers et al., "A model for the prediction of Nb_3Sn critical current as a function of field, temperature, strain, and radiation damage", *IEEE Trans. Magn.*, vol. 27, no. 2, Mar 1991, pp. 2041 – 2044.
[12] E. Barzi et al., "Study of Nb_3Sn strands for Fermilab's high field dipole models", *IEEE Trans. Appl. Supercon*., vol.11, no.1, March 2001, pp. 3595 - 3598.
[13] L.J. Vieland and A.W. Wicklund, "Specific heat of niobium-tin", *Physical review*, vol. 166, no. 2, February 1968, pp. 424-431.
[14] T. C. Cetas et al., "Specific Heats of Cu, GaAs, GaSb, InAs, and InSb from 1 to 30°K", *Phys. Rev.*, vol. 174, no. 3, October 1968, pp. 835-844.
[15] R.G. Mints et al., "Current voltage characteristics and superconducting state stability in composites", *J. Phys. D*, vol. 15, no. 11, 1982, p.2297.

[16] E.Y. Klimenko et al., “Stability of SC composite at rapid current charging and against pulsed heating”, *IEEE Trans. Magn*., vol. 24, no. 2, March 1988, pp.1167-1169.
[17] R. Yamada, *private communication*.
[18] E. Barzi et al., “Study of Current Carrying Capability of Nb_3Sn Cables in Self-field Using a SC Current Transformer”, *submitted for publication at this conference*.
[19] G. Ambrosio et al., “Critical Current Measurement of Nb_3Sn Rutherford-type Cables for High Field Accelerator Magnets”, *submitted for publication at this conference*.
[20] A.V. Zlobin et al., “Development and Test of Nb_3Sn Cos-theta Dipoles Based on PIT Strands”, *submitted for publication at this conference*.